Cross-Comparison of Brain Metabolomic Profile in Two Mouse Models of High Sleep Pressure, and Pharmacologic Analysis of Metabolites Associated with High Sleep Pressure

（２つの高睡眠圧マウスモデル間の脳メタボロームの交差比較と、共通変動した代謝物の薬理学的効果の検討）

2021

筑波大学 グローバル教育院
School of Integrative and Global Majors in University of Tsukuba
Ph.D. Program in Human Biology

Haruka SUZUKI-ABE

筑波大学

University of Tsukuba

博士　（人間生物学）学位論文

PhD dissertation in Human Biology

Table of Contents

Abstract

Sleep, or sleep-like behavior, is regulated by an interaction between two processes called the homeostatic and the circadian processes. Sleep pressure, the driving force of the homeostatic process, is accumulated during wakefulness and dissipated during sleep. Sleep deprivation has been used to investigate the molecular substrate of sleep pressure; however, sleep deprivation induces changes not only reflecting increased sleep pressure but also reflecting inevitable stresses and prolonged wake state itself. We recently reported established novel mutant mice named *Sleepy* which exhibit constitutively high levels of sleep pressure despite sleeping longer.

Here, multivariate analyses and a cross-comparison of brain metabolomic profiles were performed between ad lib slept wildtype versus sleep-deprived wild-type mice (SD), as well as wild-type mice versus *Sleepy* mutant mice, to screen for brain metabolite changes associated with increased sleep pressure. Targeted metabolome analyses of whole brains quantified 203 metabolites in total, of which 43 metabolites showed significant changes in SD, and 3 were significantly changed in both hetero/homozygous *Sleepy* mutant mice. The cross-comparison revealed a metabolite, betaine, and a metabolite group, imidazole dipeptides, to be commonly changed in both high sleep pressure models. These metabolites may be novel markers of sleep pressure at the whole-brain level. Furthermore, the present study demonstrated that intracerebroventricular injection of imidazole dipeptides increased NREM sleep time, suggesting the possibility that imidazole dipeptides may participate in the sleep regulation in response to elevated homeostatic sleep pressure through a potential novel signaling pathway.

Abbreviations

3mHMC	3-methyl-homocarnosine
aCSF	artificial cerebrospinal fluid
β-Ala	beta-alanine
CAR	Carnosine
EEG	Electroencephalography
EMG	Electromyography
FDR	False discovery rate
GABA	γ-aminobutyric acid
GC-MS	Gas chromatography-mass spectrometry
His	Histidine
HMC	Homocarnosine
ICV	Intracerebroventricular
LC-MS	Liquid chromatography-mass spectrometry
NREMS	Non-rapid eye movement sleep
PCA	Principal component analysis
PLS-ROG	Partial least squares with rank order of groups
REMS	Rapid eye movement sleep
SD	Sleep deprivation, or Sleep-deprived
Sik3	Salt-inducible kinase 3
Slp	*Sleepy* (mutant mouse)
ZT	Zeitgeber Time

Introduction

Sleep, or sleep-like behavior, is a widely preserved resting behavior in the Animalia kingdom (Hendricks et al., 2000; Nath et al., 2017; Raizen et al., 2008; Yokogawa et al., 2007). In mammals, sleep is regulated by an interaction between two processes, called Process S: the homeostatic sleep process, and Process C: the circadian processes (Borbély, 1982; Borbély et al., 2016). Process S is driven by a homeostatic sleep pressure, which is also called sleep need. The sleep pressure is gradually accumulated while animals stay awake and dissipated while they sleep (Franken et al., 2001; Suzuki et al., 2013). The regulation of the homeostatic sleep pressure is thought to involve widespread neural cell types and brain regions (Thompson et al., 2010; Vyazovskiy and Harris, 2013), whereas specific and local neural circuits execute transitions between sleep/wake states (Saper and Fuller, 2017).

To study increased homeostatic sleep pressure in animals, animals were disturbed by their sleep for hours. This experiment is called sleep deprivation (SD) and has been the only method to study sleep pressure for centuries (Bentivoglio and Grassi-Zucconi, 1997). Delta power (1–4 Hz) of electroencephalography (EEG) during non-rapid-eye-movement sleep (NREMS) has been reported as the most reliable marker of sleep pressure, since it is enhanced with the length of time of experiencing SD and declined to the normal level after recovery sleep, which is a rebound of forced wakefulness (Bjorness et al., 2016). Previous omics analyses using SD experiments have revealed that certain RNA, proteins, and metabolites were associated with high sleep pressure (Goel, 2015; Wang et al., 2018). SD, however, has a severe technical

limitation: the results after SD are contaminated with effects not only of the increased sleep pressure but also of the forced wakefulness and the physical/psychological stress.

As another distinct novel model of high sleep pressure in mice, Funato et al previously reported a mutant mouse pedigree named *Sleepy*. The main phenotype of the mutant mice is constitutively high sleep pressure although they spend longer NREMS time than wild-type mice (Funato et al., 2016). In *Sleepy* mice, there is a dominant mutation resulting in the loss of exon 13 of the *Sik3* gene, a member of the AMP-activated protein kinase family.

Here, two distinct mouse models of high sleep pressure, SD and *Sleepy,* are available. Using the whole brains of these two mice, Wang et al previously conducted a quantitative phosphoproteomic analysis and found that both mice brains showed a similar pattern of phosphorylation on synaptic proteins (Wang et al., 2018). Therefore, with similar logic, I hypothesized that a cross-comparison of the metabolomic profiles of two models would screen for common metabolite changes that are associated with increased sleep pressure. In addition, I also hypothesized that, if these metabolomic changes are not merely epiphenomena coordinating with the increased sleep pressure, the quantitative change of the brain metabolites with pharmacologic administration may affect sleep/wakefulness and/or reproduce the condition with enhanced/dissipated sleep pressure.

The contents of this dissertation were already published as a part of the following research article (Suzuki-Abe et al., 2021)

Material and Methods

Animals

All animals were maintained following procedures which were approved by the Institutional Animal Care and Use Committee of University of Tsukuba. C57BL/6N was the background of all wild-type and *Sleepy* male mice used in this study. For injection studies, male C57BL/6N mice were provided from CLEA Japan. All mice were maintained under humidity and temperature-controlled conditions (22–25±1°C) with a 12-h light-dark cycle. Food and water were provided to all mice ad libitum. For the SD experiments, mice were deprived of their sleep by gentle handling for 6 h from Zeitgeber Time (ZT) 0 as described in a previous study (Suzuki et al., 2013). All mice were sacrificed by cervical dislocations without anesthesia to collect the brain at ZT6 for further molecular biological experiments.

Brain sample preparation for metabolomics

After the cervical dislocation, mouse brains were quickly dissected into half hemispheres and frozen in liquid N2 within 40-60 s. Metabolites from the brain were extracted with the method as follows. Tissue blocks were added to 800 μl of a mixture of solvent (methanol: water = 4:1) with 6 μl of 0.1 mg/ml 2-isopropylmalic acid (Sigma-Aldrich). 2-isopropylmalic acid was utilized as an internal standard for GC-MS analysis. Then, the mixture was homogenized in a homogenizer (Micro Smash MS-100R, TOMY) with 2 mm diameter of zirconia beads. After the homogenized samples were centrifuged at 16,000 x g for 30 m at 25°C, 600 μl of supernatant was collected. The supernatant was mixed with 250 μl of purified water and 400 μl of chloroform by a

vortex mixer for 30 s. After centrifuging the suspension at 2,000 g for 10 min at 25°C, the upper aqueous phase was separated into four aliquots (each volume of 150 μl). Each aliquot was evaporated with a vacuum concentrator (CVE-3100, EYELA) for further GC-MS and LC-MS analyses.

Gas chromatography-mass spectrometry (GC-MS) analysis

The dried sample after the evaporation was dissolved into 40 μl of methoxyamine solution (20 mg/ml in pyridine, Sigma-Aldrich) and mixed at 1200 rpm for 30 min at 37°C. For trimethylsilyl derivatization, 20 μl of N-methyl-N-trimethylsilyl trifluoroacetamide solution (GL science) were added, and agitated at 1200 rpm for 30 min at 37°C. After centrifugation, 50 μl of supernatant was transferred into a glass vial for GC-MS measurement with a GCMS-TQ8050 (Shimadzu). The derivatized metabolites were separated on a BPX-5 column (30 m x 0.25 mm internal diameter, film thickness 0.25 mm, SGE). The flow rate of the helium carrier gas was set at 39 cm/s. The inlet temperature was set as 250°C and the column temperature was first held at 60°C for 2 min, then raised at the rate of 15°C/min to 330°C, and then held for 3 min. Into the GC-MS, 1 μl of the sample was injected in the split mode (split ratio 1:30). The mass spectra were obtained under the following conditions: electron ionization (ionization voltage 70 eV), ion source temperature 200°C, interface temperature 250°C. Multiple reaction monitoring (MRM) modes were based on the Smart Metabolites Database (Shimadzu). For semi-quantitative analysis, the area under the curve of each metabolite peak was calculated and divided by the area under the curve of the internal standard peak.

Liquid chromatography-mass spectrometry (LC-MS) analysis

The dried sample was reconstituted with 100 µl of 0.1% formic acid-water. 4 µl of each sample was injected into a coupled system of a Nexera UHPLC system and LCMS-8060 (Shimadzu), a triple-quadrupole mass spectrometer. COSMOSIL PBr column (2.0 mm internal diameter x 150 mm, 5µm particle, Nacalai Tesque) was used for the chromatographic separation with mobile phase A (0.1% formic acid-water) and mobile phase B (0.1% formic acid-acetonitrile). A gradient program was as follows: 0-3 min, 0% B; 3-15 min, 0% B to 60% B; 15-17.5 min, 95% B; 17.5-20 min, 95% B to 0% B, 20-24 min, 0% B. The total flow rate was 0.2 ml/min, and the column oven temperature was maintained at 40˚C. LCMS-8060 was operated in positive and negative ion modes. Parameters were as follows: desolvation line temperature, 250 ˚C; block heater, 400 ˚C; nebulizing gas flow, 3 µl/min; dying gas flow, 10 µl/min; heating gas flow, 10 µl/min. MRM measurement conditions were optimized by flow injection analysis with each standard solution.

Metabolome data analysis

Auto-scaling (normalized to be mean: 0, and standard deviation: 1) was used for the normalization of peak intensity acquired with GC/LC-MS. Some metabolites with 2 > missing values were excluded from the analysis, and no missing values were estimated. Multivariate analyses were performed with the normalized values as follows: principal component analysis (PCA), on the web browser application MetaboAnalyst (Chong et al., 2019; Pang et al., 2021); partial least squares with rank order of groups (PLS-ROG) analysis (Yamamoto, 2017), R code published in Github (Yamamoto, 2019). For

circadian analysis in Figure 3b, the original raw peak intensity table of detected metabolites was obtained from a previous study (Dyar et al., 2018). The mean of the peak intensity of metabolite in interest was normalized to 1 as the original article performed (Dyar et al., 2018) for the following analysis. Missing values were estimated using the feature-wise k-Nearest Neighbors algorithm on the MetaboAnalyst. The oscillation was analyzed with JTK_cycle, an algorithm designed to efficiently identify and characterize cycling variables (Hughes et al., 2010), using the normalized values.

Electrode and cannula implantation surgery

Surgery was conducted as previously described with minor modifications (Iwasaki et al., 2018; Miyoshi et al., 2019). Surgeries were performed on male mice, aged 8-14 weeks, under anesthesia with isoflurane (4% for induction for 5 m, 2% for maintenance) for implantation of intracerebroventricular (ICV) cannula and electroencephalography/electromyography (EEG/EMG) electrodes with 4 EEG electrode pins and 2 flexible Teflon-coated stainless EMG wires. A guide cannula was made with a 23-gauge stainless tube and inserted with a stereotaxic control, which was tilted 30° to the sagittal plane. The 30° tilting was for providing a space for the electrode attachment. The tip of the cannula was targeted to the right lateral ventricle. The stereotaxic coordinate was as follows: anteroposterior (AP): −0.50 mm, mediolateral (ML): 1.00 mm, and dorsoventral (DV): −2.25 mm. The implantation of EEG/EMG electrodes was followed immediately after cannula implantation. The electrode pins were positioned over the frontal and occipital cortices. The 4 EEG electrode pins coordinated AP: 0.5 mm, ML: 1.77 mm, DV: −1.3 mm; and AP: −4.5 mm, ML: 1.77 mm, DV: −1.3 mm. Dental cement (3M ESPE, Ketac Cem Aplicap) was used for fixing

the guide cannula and EEG/EMG electrodes on the mouse skull. Dummy cannulas, made with 30-gauge stainless tubes, were kept inserted into the guide cannulas as a cap except when the ICV injections were performed. The two stainless wires were inserted into the trapezius muscles for EMG recording.

EEG/EMG recording and analysis

All mice rested for at least 7 days to recover from the surgery. After the recovery, a tether cable was connected to electrodes on each mouse head, and then they spent additional 7 days acclimating to recording conditions. During the acclimation period, each mouse was singly housed in a recording cage in a recording room under a 12h light/dark cycle with a constant room temperature (24–25 °C). After the acclimation was finished, the EEG/EMG signals were recorded for basal sleep/wake pattern were recorded for 2 consecutive days from ZT 0, and then the sleep/wake pattern after pharmacologic administration was also recorded (for the detailed schedule, see the next section *ICV injection*). The EEG/EMG data were visualized and semi-automatically analyzed by MATLAB-based software, called SleepyScore and developed for usage in the author's laboratory, and partially corrected by visual inspections of the author. The sleep/wake state was determined into non-rapid eye movement sleep (NREMS), REMS, or wakefulness in each 20-s epoch time window. The criterion of each sleep/wake stage was as follows: Wakefulness: the presence of fast EEG, high amplitude, and variable EMG; NREMS: high amplitude, delta (1–4 Hz) frequency EEG and low EMG tonus; and REMS: theta (6–9 Hz)-dominant EEG and EMG atonia. The total amounts of time spent in each state were calculated by summing the total number of 20-s epochs in each state. Using MATLAB-based custom software, EEG signals were subjected to short-

time Fourier transform analysis from 1 to 30 Hz with 1-Hz bins. For normalization of the EEG power density, EEG power in each frequency bin was expressed as a percentage of the mean EEG power in all frequency ranges (1–30 Hz). Delta density during NREMS was calculated as the ratio of delta power (1–4 Hz) to total EEG power (1–30 Hz) at each 20-s epoch.

ICV Injection

Handling of every mouse for ICV injection without anesthesia was performed for 5 mins at least once every other day during the 7 days of acclimation to the tether and recording environment. After the recording of baseline sleep/wake pattern for 2 consecutive days, 2 μl of artificial cerebrospinal fluid (aCSF: 125 mM NaCl, 2.5 mM KCl, 1.25 mM NaH_2PO_4, 26 mM $NaHCO_3$, 10 mM glucose, 2 mM $CaCl_2$, and 1 mM $MgCl_2$) were injected to mice as vehicle control without anesthesia through the guide cannula using a 5-μl syringe (Hamilton #85) at the indicated ZT. Each ICV injection was performed within 5 min and the procedure was as follows: 1 min for 2 μl injection, 1 min for holding to prevent backflow of injected aCSF, and the remaining time for removal/re-insertion of dummy cannula for capping and dis-/re-connection of tether with the recording cable. Between the injections of the vehicle and the first tested compound, every mouse took at least 1-day rest. Between compound injections, they took 3-day washout periods. I set the concentrations of tested compounds based on the absolute amount of the metabolites in the previous study since the present metabolome analysis did not perform the absolute quantification of each metabolite. Jain et al quantified the amount of carnosine in the mouse whole brain as 20 ng/mg. Therefore, with an estimation of the weight of a mouse to be 400 mg, the total amount of carnosine

in a mouse brain would be estimated as 8 μg/brain. The fold change of carnosine was 1.22 to 1.25 (Figure 1c) in the present metabolome analysis. To mimic the fold changes, I injected 2μl of 5mM (2.26 μg) carnosine with the ICV injection, and followed the same concentration in the other ICV injections as well.

Statistics

Prism 9 (GraphPad) was mainly used to perform statistical analyses. In addition, some additional software or tools were used for some specific analysis as follows: MetaboAnalyst (Chong et al., 2019; Pang et al., 2021) for metabolomic analysis; R for JTK-cycle (Hughes et al., 2010) and PLS-ROG (Yamamoto, 2017); and SPSS Statistics 26 (IBM) for non-parametric analyses. For multiple comparisons with multiple data points, one-way repeated-measures ANOVA was used, and for multiple comparisons involving two independent variables, two-way ANOVA was used. ANOVA tests were followed by Dunnet's or Tukey's test for multiple comparisons up to the assumption of equivariance. For non-parametric comparisons of two groups, the Wilcoxon rank sum t-test was used. False Discovery Rate (FDR) adjustment was basically performed by the two-stage linear step-up procedure of Benjamini, Krieger and Yekutieli. For the EDR adjustment of the result with JTK_cycle, the Benjamini-Hochberg method was used due to the R program design.

Results

Metabolomic changes associated with increased sleep pressure

To identify metabolomic changes associated with high sleep pressure, targeted metabolome analyses with a combination of LC-MS and GC-MS were performed using the whole-brain lysates. I conducted two sets of metabolome analyses: 1) I compared wild-type littermate brains (+/+) with heterozygous and homozygous *Sleepy* mutant brains (*Slp*/+, *Slp*/*Slp*); and 2) I compared 6-h ad lib slept brains (ad) with 6-h SD wild-type brains (SD) (Figure 1a). All mice were sacrificed at ZT 6 at the same timing as the end of SD, in order to control for the metabolomic changes due to circadian rhythms (Dyar et al., 2018).

203 metabolites were quantified through the present metabolome analyses. I performed multivariate analyses to screen for the metabolites that cluster the mice reflecting the levels of sleep pressure. Firstly, principal component analysis (PCA), the most used unsupervised analysis, was performed. PCA did separate the SD and ad based on sleep pressure, however, PCA did not separate wild-type littermate mice and *Sleepy* mutant mice (Figure 1b-c, and Table 1). Therefore, I additionally performed supervised multivariate analysis. I chose the partial least square-rank of group (PLS-ROG) analysis among various types of PLS analysis, which is a widely used supervised analysis in the field of metabolomics. PLS-ROG analysis has two advantages compared to other types of PLS methods: 1) PLS-ROG can distinguish groups not only by the sample sets merely but also by reflecting the rank order of sample sets, i.e., in this study, the level of sleep pressure; 2) PLS-ROG, like PCA, enables to screen for the metabolites significantly correlated with the interested “axis” by statistical hypothesis testing of

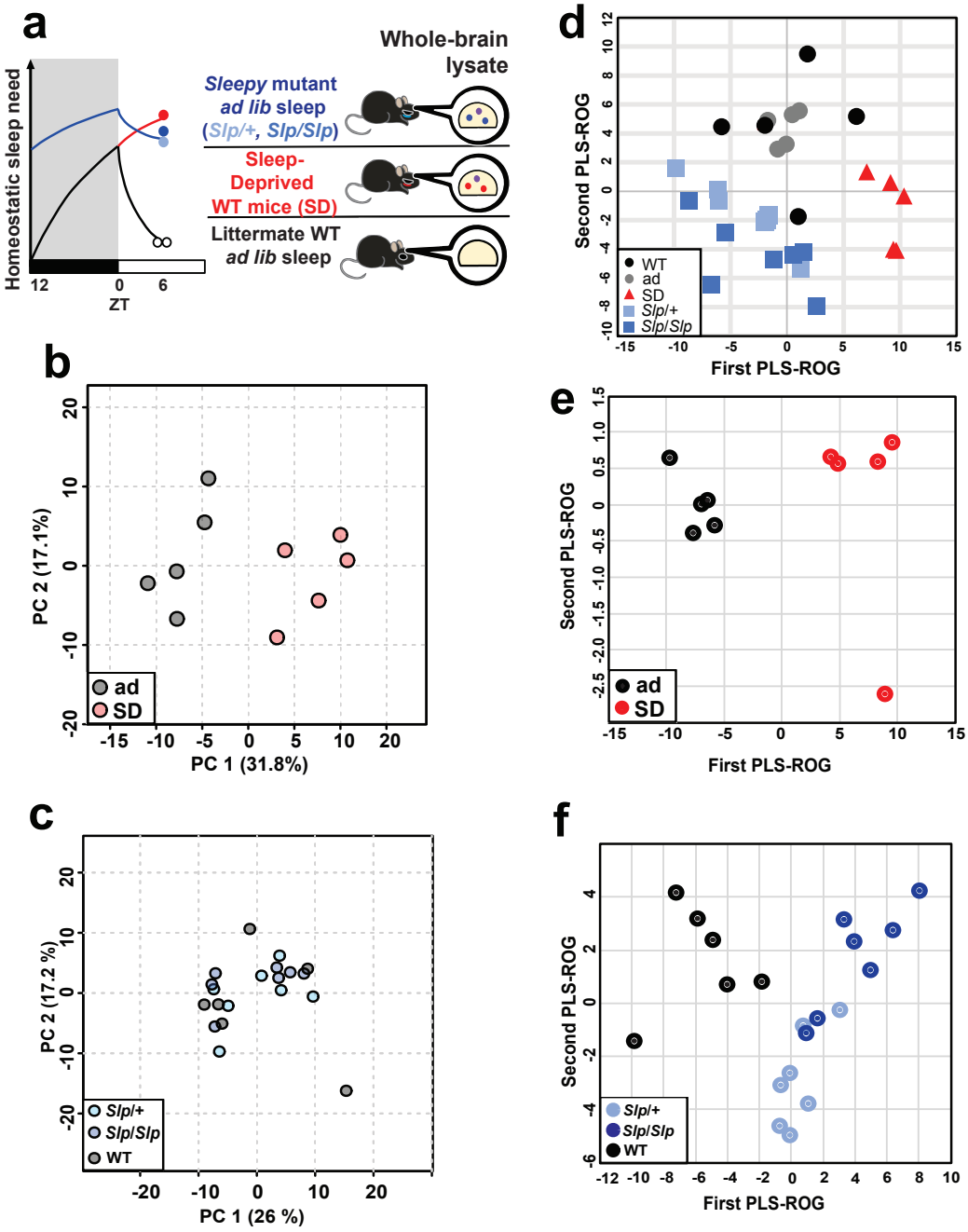

Figure 1. Multivariate analysis using two distinct mouse models of high sleep pressure.

(a) Experimental design for metabolome analyses in two mouse models of elevated sleep pressure.

(b) PCA for ad lib slept mice (ad) versus SD mice. ad: littermate wild-type of SD mice (n = 5), SD: sleep-deprived mice (n = 5). For metabolites correlated with PC1, see Table 1.

(c) PCA for wild-type mice (WT) versus *Sleepy* mice. WT: littermate wild-type of *Sleepy* mice (n = 5), *Slp/+*: *Sleepy* heterozygous mice (n = 7), and *Slp/Slp*: Homozygous mice (n = 7). No table is available.

(d) PLS-ROG analysis for metabolites associated with high sleep pressure. For metabolites correlated with 2nd PLS-ROG, see Table 2.

(e) PLS-ROG analysis for ad versus SD. For metabolites correlated with 1st PLS-ROG, see Table 3.

(f) PLS-ROG analysis for WT versus *Sleepy* mice. For metabolites correlated with 1st PLS-ROG, see Table 4.

Table 1.
List of metabolites significantly correlated with PC1 (Supplemental Figure 1a, x-axis) of PCA in the comparison of ad lib slept mice and SD mice.

	R	*p* -value		R	*p* -value		R	*p* -value
Arabinonic acid	-0.914	**0.00022**	Lactitol	0.839	**0.0024**	3-Hydroxybutyric acid	0.758	**0.011**
Phosphoric acid	-0.905	**0.00031**	Putrescine	-0.833	**0.0027**	O-phosphoethanolamine	-0.755	**0.012**
2-Hydroxybutyric acid	0.904	**0.00033**	Glutaric acid	0.832	**0.0029**	Lysine	-0.751	**0.012**
Tryptophan	0.900	**0.00039**	PropionylcarnitineC3	0.831	**0.0029**	2-Aminobutyric acid	0.743	**0.014**
Glycolic acid	0.890	**0.00056**	Cystathionine	-0.830	**0.0030**	2-Aminoadipic acid	0.736	**0.015**
Betaine	-0.876	**0.00089**	Phenylalanine	0.829	**0.0030**	Tyrosine	-0.731	**0.016**
3-Hydroxyisobutyric acid	0.875	**0.00092**	Serine	-0.827	**0.0032**	Threonic acid	-0.726	**0.017**
5-HIAA	0.870	**0.0011**	Threonine	-0.826	**0.0032**	N-Acetylhistidine	-0.722	**0.018**
Gluconic acid	0.870	**0.0011**	Phenyllactic acid	0.825	**0.0033**	NADP	-0.718	**0.019**
NAD	-0.866	**0.0012**	2-Phosphoglyceric acid	-0.817	**0.0039**	Adenosylmethionine	0.718	**0.019**
Glyceric acid	-0.865	**0.0012**	Citrulline	-0.816	**0.0040**	Dimethylglycine	-0.712	**0.021**
Arabinose	-0.865	**0.0012**	**Homocarnosine**	0.814	**0.0041**	Taurine	-0.709	**0.022**
3-Aminoisobutyric acid	0.860	**0.0014**	Sarcosine	-0.810	**0.0045**	Uric acid	0.705	**0.023**
Kynurenine	0.859	**0.0015**	Spermidine	0.809	**0.0046**	3-Hydroxykynurenine	0.698	**0.025**
2-Methylbutyrylcarnitine	0.858	**0.0015**	Fructose 1-phosphate	0.799	**0.0055**	4-Hydroxyproline	-0.697	**0.025**
myo-Inositol	-0.858	**0.0015**	Glutamine	-0.798	**0.0057**	Cysteine	-0.691	**0.027**
3-Phosphoglyceric acid	-0.855	**0.0016**	DOPAC	0.794	**0.0061**	Asparagine	-0.683	**0.030**
Glycine	-0.854	**0.0017**	2-Oxoglutaric acid	-0.792	**0.0063**	Myristic acid	-0.676	**0.032**
ADP	-0.853	**0.0017**	Valine	0.787	**0.0069**	N-Acetyl-Asp-Glu	-0.673	**0.033**
IsobutyrylcarnitineC4	0.852	**0.0018**	Sorbitol	0.776	**0.0083**	Xanthosine	0.668	**0.035**
N'-Formylkynurenine	0.849	**0.0019**	Glucose 6-phosphate	0.770	**0.0092**	Ascorbic acid	-0.665	**0.036**
Indoleacetic acid	0.839	**0.0024**	Phenol	-0.770	**0.0092**	Hexanoylglycine	0.660	**0.038**
Indolelactic acid	0.839	**0.0024**	Maltose	0.759	**0.011**	Isoleucine	0.637	0.047

69 metabolites

Red: Sleep pressure associated metabolites

Bold *p*-values *q* -value < 0.05

Bold *p*-values *q* -value < 0.1

Table 2: Metabolites correlated with 2nd PLS-ROG (Figure 1b y-axis; sleep pressure)

Metabolites	R	*p* -value	*q* -value
Betaine	-0.810	**0.00000006**	**0.000012**
Acetylcarnosine	0.633	**0.00017**	**0.013**
Glycolic acid	0.632	**0.00018**	**0.013**
Carnosine	0.615	**0.00030**	**0.015**
Pipecolinic acid	0.609	**0.00035**	**0.015**
4-Hydroxyproline	-0.579	**0.00081**	**0.028**
Acetylornithine	0.573	**0.0009**	**0.028**
Sorbitol	0.562	**0.0012**	**0.033**
Gluconic acid	0.539	**0.0021**	**0.050**
Homocarnosine	0.500	**0.0049**	**0.10**
DOPAC	0.468	**0.0091**	0.18
Hypotaurine	-0.456	**0.011**	0.2018

Red: *q* -value < 0.1

Table 3:
List of metabolites significantly correlated with 1st PLS-ROG (Supplemental Figure 1c, x-axis) in the comparison of ad lib slept mice and SD mice.

	R	*p*-value		R	*p*-value		R	*p*-value
3-Hydroxyisobutyric acid	0.970	**0.0000033**	Glyceric acid	-0.813	**0.0043**	Uric acid	0.711	**0.021**
3-Aminoisobutyric acid	0.955	**0.000017**	Lysine	-0.809	**0.0046**	**Homocarnosine**	0.709	**0.022**
N'-Formylkynurenine	0.920	**0.00016**	2-Aminoadipic acid	0.804	**0.0051**	Phenol	-0.703	**0.023**
Isobutyrylcarnitine(C4)	0.919	**0.00017**	Fructose 1-phosphate	0.802	**0.0052**	Gluconic acid	0.699	**0.025**
Putrescine	-0.918	**0.00018**	Threonine	-0.801	**0.0054**	2-Phosphoglyceric acid	-0.698	**0.025**
2-Hydroxybutyric acid	0.914	**0.00021**	Isoleucine	0.788	**0.0068**	Spermidine	0.691	**0.027**
Valine	0.904	**0.00033**	Hexanoylglycine	0.784	**0.0073**	2-Oxoglutaric acid	-0.680	0.031
Kynurenine	0.903	**0.00035**	Phenylalanine	0.779	**0.0079**	Aspartic acid	0.675	0.032
2-Methylbutyrylcarnitine (C5)	0.899	**0.00040**	Tyrosine	-0.774	**0.0085**	NAD	-0.674	0.033
5-HIAA	0.897	**0.00043**	N-Acetylhistidine	-0.771	**0.0091**	Citrulline	-0.670	0.034
Tryptophan	0.888	**0.00061**	Glycine	-0.758	**0.011**	3-Hydroxykynurenine	0.668	0.035
3-Hydroxybutyric acid	0.882	**0.00073**	**Betaine**	-0.755	**0.012**	Trigonelline	-0.664	0.036
Arabinonic acid	-0.868	**0.0011**	Cystathionine	-0.755	**0.012**	Sorbitol	0.660	0.038
Phenyllactic acid	0.850	**0.0019**	Pantothenic acid	-0.748	**0.013**	Xanthosine	0.659	0.038
Arabinose	-0.846	**0.0020**	Phosphoric acid	-0.746	**0.013**	Serine	-0.656	0.039
Glycolic acid	0.845	**0.0021**	ADP	-0.738	**0.015**	1-Methylhistidine	0.650	0.042
2-Aminobutyric acid	0.841	**0.0023**	DOPAC	0.734	**0.016**	Threonic acid	-0.649	0.042
Lactitol	0.838	**0.0025**	Pipecolinic acid	0.734	**0.016**	Acetylornithine	0.647	0.043
Indolelactic acid	0.833	**0.0027**	Glucose 6-phosphate	0.732	**0.016**	Margaric acid	-0.646	0.044
Indoleacetic acid	0.827	**0.0032**	3-Phosphoglyceric acid	-0.722	**0.018**	Sarcosine	-0.643	0.045
Propionylcarnitine (C3)	0.818	**0.0038**	myo-Inositol	-0.721	**0.019**	2-Aminoethanol	-0.635	0.049
Glutaric acid	0.816	**0.0040**	Maltose	0.714	**0.020**	Glutamine	-0.632	0.050

Red: Sleep pressure associated metabolites

66 Metabolites

Bold *p*-values *q*-value < 0.05

Bold *p*-values *q*-value < 0.1

Table 4:
List of metabolites significantly correlated with 1st PLS-ROG (Supplemental Figure 1d, x-axis) in the comparison of wild-type mice and *Sleepy* mice.

	R	*p* -value		R	*p* -value
Betaine	-0.859	**0.0000013**	Glutamine	0.544	0.013
Acetylcarnosine	0.818	**0.000011**	Hexanoylcarnitine(C6)	-0.535	0.015
Carnosine	0.746	**0.00016**	2-Hydroxyglutaric acid	-0.532	0.016
Pipecolinic acid	0.720	**0.00035**	DOPAC	0.520	0.019
Ascorbic acid	0.663	**0.0014**	Gluconic acid	0.505	0.023
3-Hydroxybutyric acid	-0.638	**0.0025**	Acetylornithine	0.491	0.028
Indoleacetic acid	0.636	**0.0026**	Dopamine	0.489	0.029
Histamine	0.626	**0.0032**	Pantothenic acid	0.486	0.030
Glycolic acid	0.588	0.0063	Fructose	0.465	0.039
Sorbitol	0.559	0.010	Thymidine	-0.460	0.041
1,5-Anhydro-D-sorbitol	-0.555	0.011	2-Hydroxy-3-methylvaleric acid	0.453	0.045
4-Hydroxyproline	-0.544	0.013			

23 metabolites

Red: Sleep pressure associated metabolites

Bold *p* -values *q* -value < 0.05

Bold *p* -values *q* -value < 0.1

factor loadings (Yamamoto et al, 2014; Yamamoto, 2017). As a result, PLS-ROG clustered the mouse groups based on sleep pressure (Figure 1d). 11 metabolites significantly correlated with the second PLS-ROG score (y-axis in Figure 1d, reflecting sleep pressure) when the two sets of metabolomic data were combined (Table 2). These same 11 metabolites were also detected in PLS-ROG without combining data (Figure 1e-f, Table 3-4).

3 metabolites, carnosine (β-alanyl-l-histidine, CAR), acetylcarnosine, and betaine (also known as trimethylglycine), were significantly altered in the comparison of *Sleepy* versus wild-type (Figure 2a). Importantly, these 3 compounds also listed in metabolites significantly correlated with sleep pressure in PLS-ROG. 43 metabolites significantly changed in the SD versus ad lib sleep mice comparison ($q < 0.1$, Wilcoxon rank sum t-test followed by FDR. Figure 2b). Out of these 43 metabolites, 4 metabolites, homocarnosine (γ-aminobutyryl-l-histidine, HMC), 3,4-dihydroxyphenylacetic acid (DOPAC), glycolic acid, and betaine (labeled in Figure 2d), also appeared among the 11 metabolites significantly correlated with the second PLS-ROG score (Figure 1d, and Table 2-4). Taken all the results together, betaine and imidazole dipeptides (dipeptides containing histidine, such as carnosine) were screened as common differential metabolites when the sleep pressure was enhanced.

To identify the impact of SD on metabolite pathways, I also performed metabolome pathway analysis using the 43 differential metabolites in SD mice. In the SD condition, 3 pathways (glycine/serine/threonine metabolism; aminoacyl t-RNA biosynthesis; valine/leucine/isoleucine biosynthesis) were significantly altered (Figure

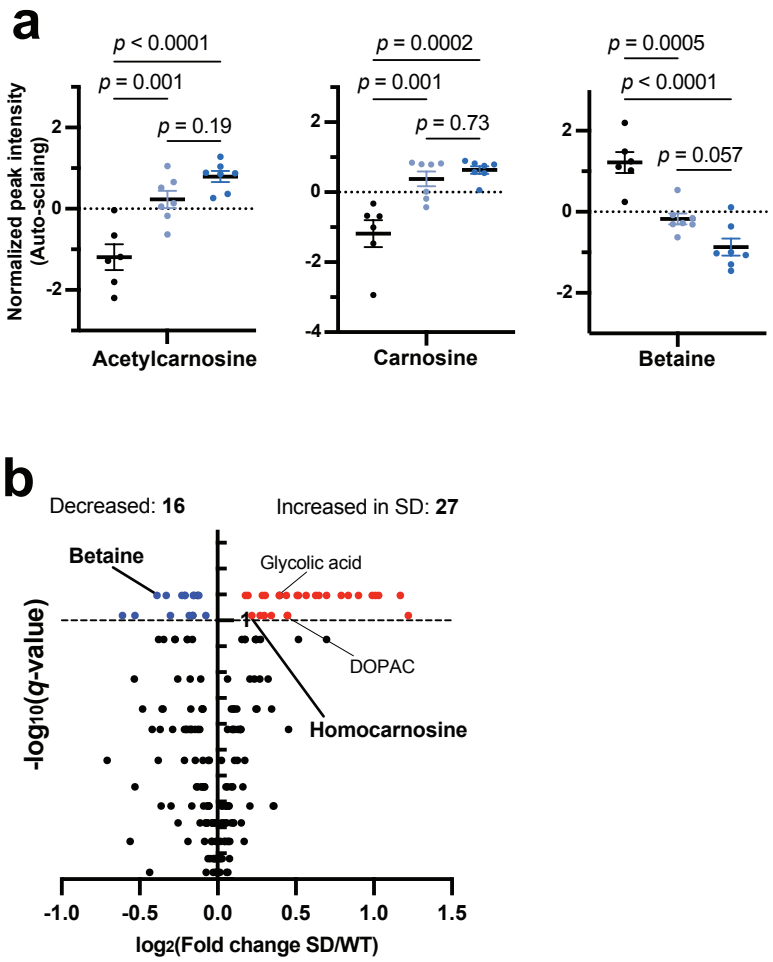

Figure 2. Differential metabolites in each mouse models with high sleep pressure.

(a) Metabolites significantly altered in *Sleepy* mice: acetylcarnosine, carnosine, and betaine. Two-way ANOVA followed by Tukey's test. Data shown as mean ± SEM.

(b) Volcano plot showing metabolomic alterations in SD mice. q < 0.1 considered significant (broken line). Wilcoxon rank sum t-test followed by FDR adjustment (two-stage linear step-up procedure of Benjamini, Krieger and Yekutieli). Four labeled markers are also listed in the metabolites correlated with y-axis of PLS-ROG analysis (see Table 2).

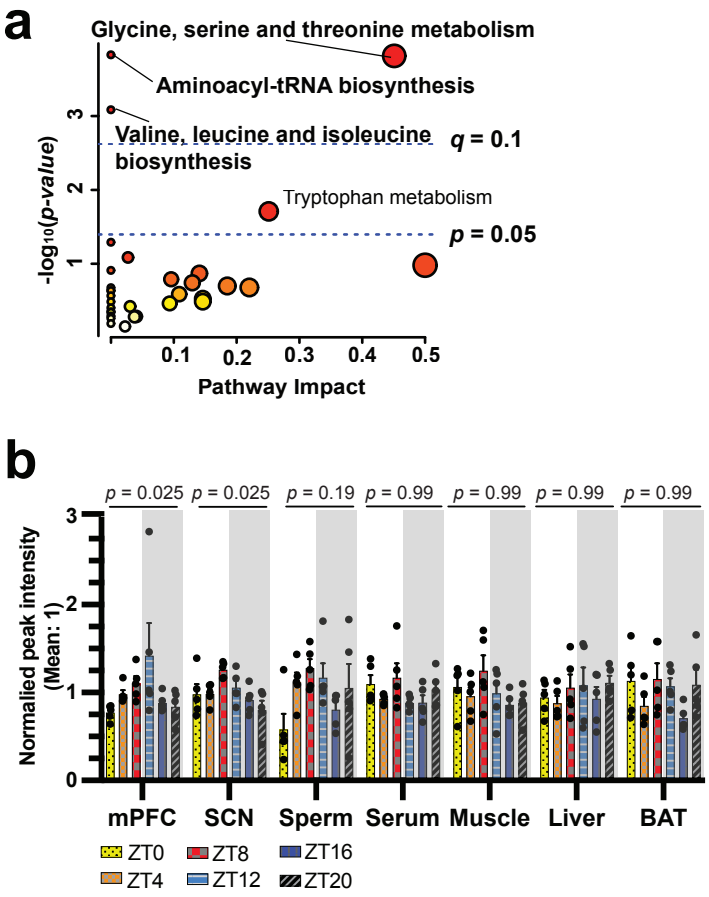

Figure 3. Further analyses using the present and previous metabolomic data sets.

(a) Metabolome pathway analysis using 43 metabolites significantly altered in SD mice. Color indicates *p* value, and circle size indicates the value of pathway impact.

(b) Circadian dynamics of betaine in mouse tissues (Dyar et al., 2018). JTK_cycle (Hughes et al., 2010) followed by FDR adjustment (Benjamini-Hochberg method). Data shown as mean ± SEM.

3a). I could not perform pathway analysis meaningfully for the comparison of *Sleepy* versus wild-type mice due to the small number of significantly altered metabolites. In addition, I reanalyzed previous metabolomic data which studied circadian dynamics of metabolites using mice multiple tissues sampled every four hours (Dyar et al., 2018). In the medial prefrontal cortex (mPFC) and the suprachiasmatic nucleus (SCN), which were all the tissues of the central nervous system used in the study, betaine showed an oscillating pattern ($p = 0.025$, and $p = 0.025$, respectively, Figure 3b). These results suggested that the betaine dynamics may reflect the daily dynamics of sleep pressure.

Pharmacologic effects of betaine and imidazole dipeptides on sleep/wake

To confirm if the changes in betaine and imidazole dipeptides are merely epiphenomena coordinating increased sleep pressure, I recorded changes in sleep/wake through EEG/EMG measurements after ICV injections of the selected metabolites.

The levels of betaine in the brain were significantly decreased when the sleep pressure is high as shown in Figure 2a and 2b. Therefore, I injected betaine to the mouse brain with high sleep pressure, i.e., SD mice and *Sleepy* mice at ZT6 (Figure 4). I expected a dissipated level of sleep pressure might be mimicked by betaine administration. However, betaine ICV injection did not affect any time spent in sleep/wake or NREM EEG delta power, a marker of sleep pressure, during the subsequent 18 h.

In contrast to the pattern of change of betaine, the imidazole dipeptides CAR and HMC in the brain were significantly elevated under high sleep pressure (Figure 2a-b). I performed ICV injection of these compounds to ad lib slept wild-type mice at ZT 11.5,

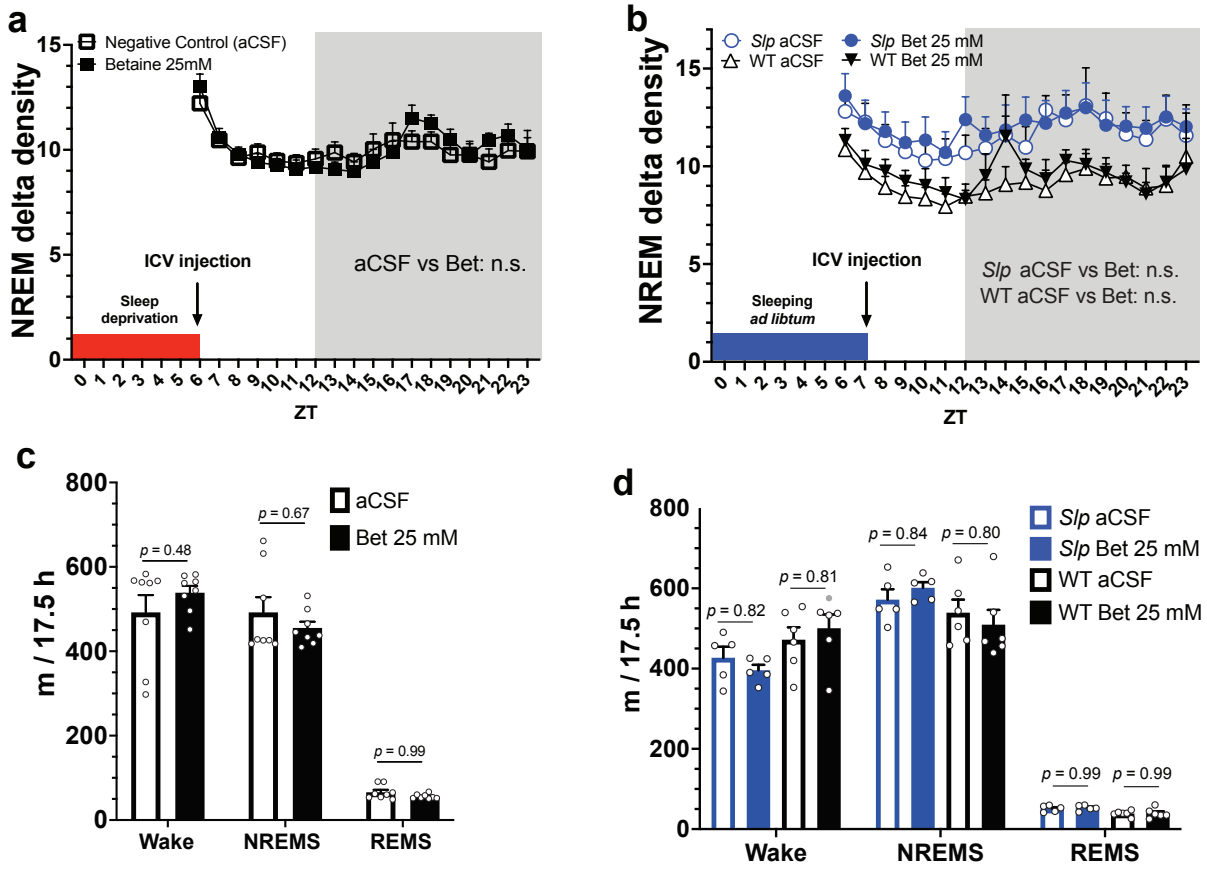

Figure 4. Pharmacologic effects of betaine on sleep/wake regulation in the mice with high sleep need, SD and *Sleepy*.

(a-b) Hourly NREM EEG delta density after ICV injection of (a) wild-type mice injected betaine at ZT6 after SD for 6 hours (n = 8), and (b) *Sleepy* mutant mice (Slp: n = 5) and littermate wild-type mice (WT: n = 6) injected betaine at ZT6 after ad lib sleep for 6 h. n.s. $p > 0.05$. Mixed-effects analysis.

(c-d) Total time of each state for 17.5 h (from ZT 6.5 to 23) after injection to (c) SD mice and (d) *Sleepy* mice.

Two-way ANOVA followed by Dunnett's test. Data shown as mean ± SEM.

when the sleep pressure became lowest (Figure 5a). I expected that the administration of imidazole dipeptides would simulate an increased sleep pressure. I additionally injected 3-methyl-homocarnosine (3mHMC) to examine the importance of the imidazole side chain on the imidazole dipeptides for their pharmacologic effects. Mice injected either of these dipeptides showed a significant decrease in time spent in wakefulness (Two-way ANOVA followed by Dunnet's test. aCSF vs HMC: $p < 0.0001$; aCSF vs CAR: $p = 0.016$; aCSF vs 3mHMC: $p = 0.012$) with a concomitant increase in time spent in NREMS (Two-way ANOVA followed by Dunnet's test. aCSF vs HMC: $p = 0.0013$, aCSF vs CAR: $p = 0.019$, and aCSF vs 3mHMC: $p = 0.024$) for 10 h during the subsequent dark phase (Figure 5b-d). There was no change in time spent in REMS (Two-way ANOVA followed by Dunnet's test. aCSF vs HMC: $p = 0.93$, aCSF vs CAR: $p = 0.99$, and aCSF vs 3mHMC: $p = 0.99$) (Figure 5b). There were no significant changes in NREMS EEG delta power, a marker of sleep pressure, (Figure 5e) or in the wake and NREMS EEG spectra through the dark phase after injection (Figure 5f and 5g).

In addition, I examined the possibility that the NREMS-inducing effect of HMC might be due to the amino acid(s) derived by hydrolysis of the dipeptide, since HMC has a side chain of γ-aminobutyric acid (GABA), a sleep-promoting inhibitory neurotransmitter in the central nervous system. GABA, histidine (His), and a 1:1 cocktail of them were injected to ad lib slept wild-type mice at ZT 11.5, when the sleep pressure is thought to be the lowest (Figure 6a). The mice injected with His or the cocktail showed a similar change of wake/sleep state as mice injected with imidazole dipeptides:

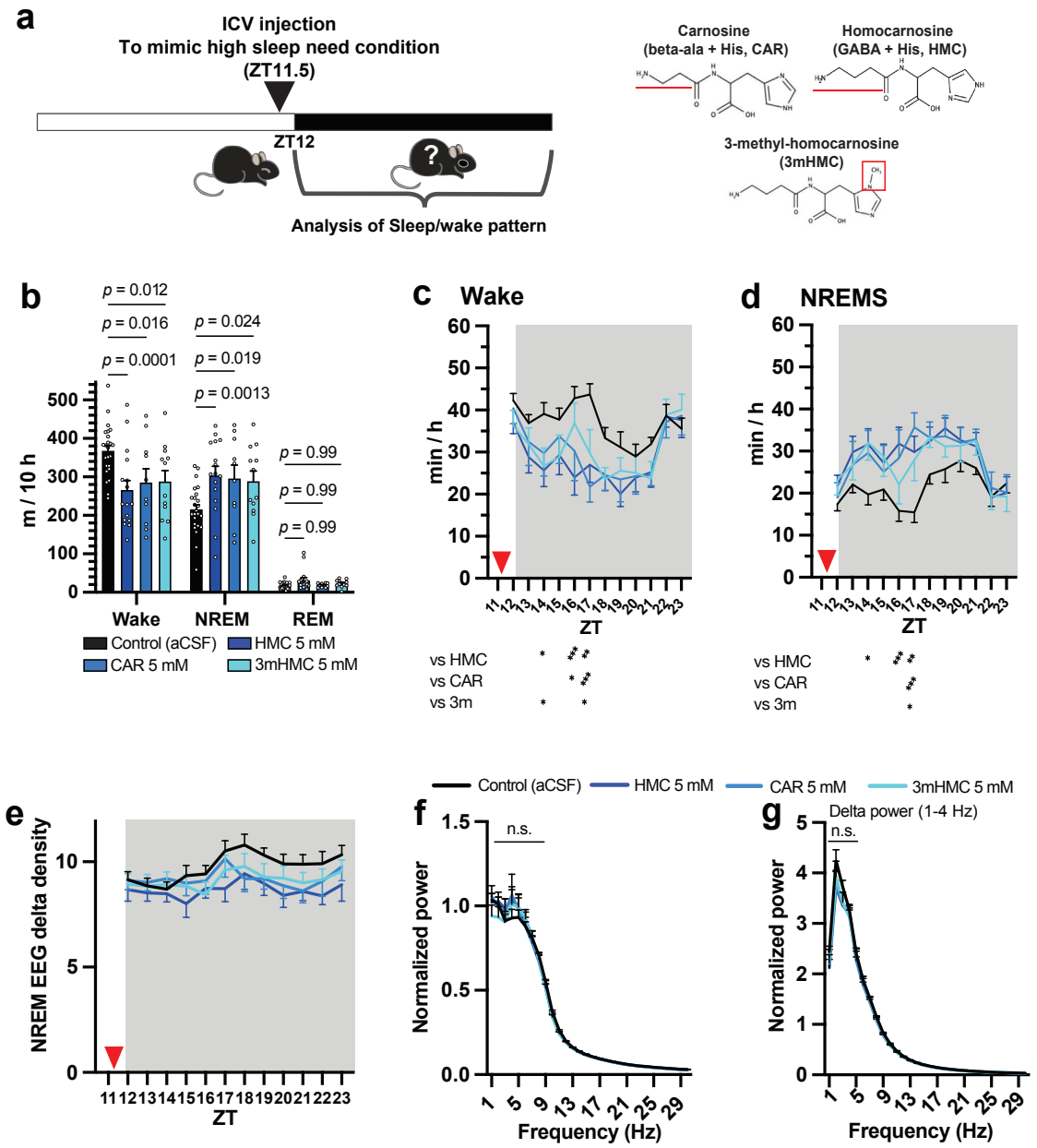

Figure 5. Pharmacologic effects of imidazole dipeptides on sleep/wake state.

(a) Experimental design for ICV injection and the chemical structures of tested dipeptides.

(b-g) Pharmacologic effects of imidazole dipeptides on sleep/wake state; aCSF (n = 24), HMC (n = 16), CAR (n = 10), and 3mHMC (n = 10).

(b) Total time of each sleep/wake state for 10 h after the injection. Two-way ANOVA followed by Dunnett's test.

(c-d) Hourly time spent in (c) Wake and (d) NREMS. * $p < 0.05$, ** $p < 0.01$, *** $p < 0.001$. Two-way ANOVA followed by Dunnett's test. Data shown as mean ± SEM. Red arrowhead indicates the timing of ICV injection.

(e) NREM EEG delta density after ICV injection.

(f-g) EEG power spectra for 12 h after injection during (f) Wake and (g) NREM. n.s. $p > 0.05$. Mixed-effects analysis. Data shown as mean ± SEM.

a significant decrease in time spent in wakefulness (Two-way ANOVA followed by Dunnett's test. aCSF vs GABA+His: p = 0.0057; aCSF vs His: p = 0.013), a significant increase in time spent in NREMS (Two-way ANOVA followed by Dunnett's test. aCSF vs GABA+His: p =0.012; aCSF vs His: p = 0.013), and no changes in time spent in REMS (Two-way ANOVA followed by Dunnett's test. aCSF vs GABA + His: p = 0.99; aCSF vs His: p = 0.99) during the 10-h subsequent dark phase after ICV injection (Fig 6b-d). Surprisingly, the GABA sole injection did not change time spent in any sleep/wake states (Two-way ANOVA followed by Dunnett's test. Wake: p = 0.86; NREMS: p = 0.88; REMS p = 0.99).

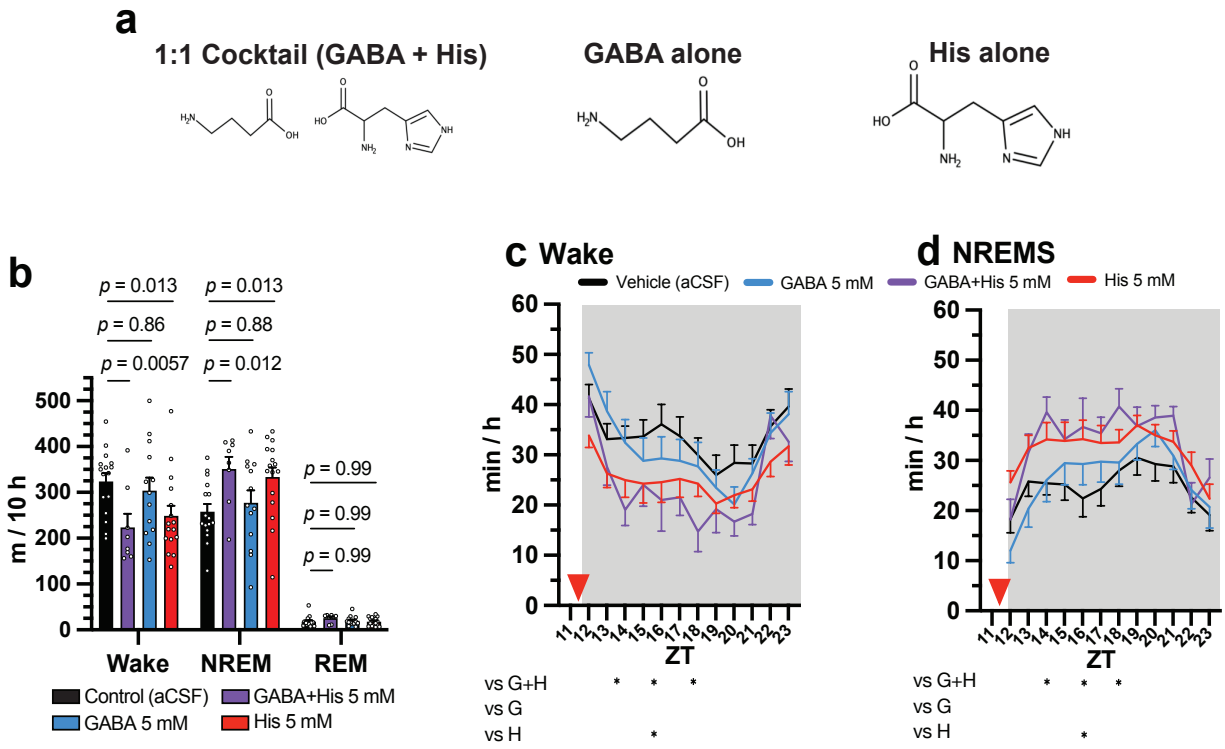

Figure 6. Pharmacologic effects of amino acids composing HMC on sleep/wake state.

(a) Chemical structures of tested amino acids.

b-d) Pharmacologic effects of amino acids on sleep/wake state in wild-type mice, Control (aCSF, n = 16), GABA+His (n = 8), GABA (n = 13), His (n = 16).

(b) Total time of each state for 10 h after the injection. Two-way ANOVA followed by Dunnett's test.

(c-d) Hourly time spent in (c) wake and (d) NREMS. * $p < 0.05$. Two-way ANOVA followed by Dunnett's test. Data shown as mean ± SEM. Red arrow head indicates the timing of ICV injection.

Discussion

Through the present study, I conducted whole-brain metabolomic analyses to identify dynamics of metabolites, whose levels altered with elevated sleep pressure. The coupling of multivariate analyses and cross-comparison of the metabolomic profiles using 2 distinct mice models with high sleep pressure clearly identified that a decrease in betaine and increases in imidazole dipeptides were associated with high sleep pressure at the whole-brain level. None of these phenomena has previously been reported to be involved in the regulation of sleep/wake state. The decrease in cerebral betaine level was also observed in the brain of human patients with schizophrenia (Ohnishi et al., 2019). Also, *Chdh* (choline dehydrogenase, a gene for betaine synthesis enzyme)-deficient mice showed a decrease in cerebral betaine level and exhibited psychiatric behaviors with schizophrenia-related molecular alterations in the brain (Ohnishi et al., 2019). Although the sleep pattern of the *Chdh*-deficient mice was not examined in the study, insomnia (or sleep disruption) is the major sleep disorder among schizophrenia human patients, especially patients with first-episode schizophrenia (Kaskie et al., 2019; Waite et al., 2020).

In the comparison of metabolomic profiles between *Sleepy* mutant and wild-type mice, only 3 out of 203 quantified metabolites showed significant changes, whereas 43 metabolites showed significant changes in the comparison between SD and ad lib slept mice. The difference suggests that the phenotypes of *Sleepy* mutant mice, physiologically increased NREMS time and sleep pressure, may not have drastic impacts on the dynamics of brain metabolites. On the other hand, the numerous alterations of metabolites found in SD mice may reflect the metabolomic changes

associated with high levels of physical and mental stress on mice accompanying the enforced wakefulness. The pathway analysis in the present study using differential metabolites in SD showed three pathway-level changes (Figure 3a), besides previous studies reported the tryptophan metabolism pathway stood out under SD conditions (well-reviewed in Bhat et al., 2020). Although it did not reach the threshold of significance with the strict criteria I used (q value < 0.1), the tryptophan metabolism pathway also showed up in the present SD analysis (Figure 3a). The change of blood tryptophan and its downstream metabolites level has been reported as a marker for physical stress (Kiank et al., 2010). Taken together, these results clearly highlight the technical limitation of using SD alone as a method to investigate the high sleep pressure; it is inevitable to filter the effects of stress from that of enhanced sleep pressure in SD animals. Moreover, no changes were observed in major neurotransmitters such as adenosine, a well-known neuromodulator involved in the Process S and sleep pressure (Bjorness et al., 2016; Lazarus et al., 2019; Peng et al., 2020) in the present cross-comparison of SD mice and *Sleepy* mutant mice. This result suggests that the homeostasis of total intracellular and extracellular amounts of neurotransmitters may be stable under high sleep pressure conditions at the whole-brain level.

In addition, I demonstrated that exogenous ICV administration of some of the differential metabolites and their components have significant pharmacologic effects on sleep/wake states. The present pharmacologic study using imidazole dipeptides, which were increased in the mouse brain with elevated sleep pressure, demonstrated a NREMS-promoting effect. The NREMS EEG delta power after the ICV injection did not change. However, the area-under-curve, or the integral, of NREMS delta power,

also termed “delta energy” which is a product of total time spent in NREMS and delta power during NREMS (Suzuki et al., 2020) and another maker of sleep pressure, was increased due to the increased NREMS time (Figure 7). This increase suggests that imidazole dipeptides could elevate the homeostatic sleep pressure in mice. The classical experiments have demonstrated that the extracts of cerebrospinal fluid from SD animals could promote NREMS when exogenously administered to ad lib slept animals (Irwin, 2019; Kubota, 1989). A series of experiments in my thesis followed a similar logic and strategy but used modern exhaustive metabolomic analyses.

The previous studies on the role of imidazole dipeptides in the rodent brain have been relatively limited. So far, 3 major roles have been studied: i) the neuroprotective effects based on their antioxidant properties (Gallant et al., 2000; Jain et al., 2020; Schön et al., 2019); ii) their involvement in the primary olfactory system due to their rich distribution in the olfactory bulb (Bonfanti et al., 1999; Burd, 1982; Wang-Eckhardt et al., 2020); and iii) their roles in signal transduction between neural and glial cells (Baslow, 2010). Although the relationship between imidazole dipeptides and mouse behavior has been little studied, carnosine dipeptidase-2 (*Cndp2*) knockout mice were reported to show abnormal sensorimotor gating, according to the International Mouse Phenotyping Consortium 2021 database (Dickinson et al., 2016). Interestingly, in chicks studies, the central administration of imidazole dipeptides rather increases the locomotor activity and times of twitters. (Furuse, 2015; Tomonaga et al., 2004; Tsuneyoshi et al., 2008). In humans, a clinical study with a small group of autistic children reported that oral administration of carnosine for 2 months improves their

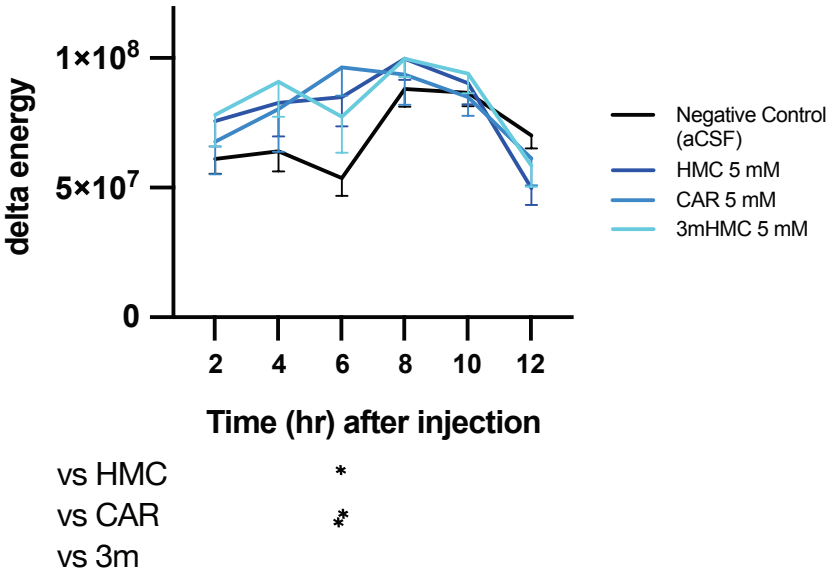

Figure 7. NREM EEG delta energy of mice after injection of imidazole dipeptides.

* $p < 0.05$, ** $p < 0.01$. Two-way ANOVA followed by Tukey's test. Data shown as mean ± SEM.

"total sleep disorders score" (Mehrazad-Saber et al., 2018). Although the detailed mechanism of action remains unclear, imidazole dipeptides may have some effects on sleep/wake state in various species of animals.

I also found that central administration of His, which is the characteristic amino acid residue of imidazole dipeptides, promoted NREMS, as well as the 1:1 cocktail of His and GABA, the two hydrolysis products of HMC did. Contrary to my expectations, ICV injection of GABA alone did not significantly change sleep/wake states in mice. GABA acts on $GABA_{A\ and\ B}$ classes of receptors, whose activation is known to promote sleep (Gottesmann, 2002). The negative results presented here might be due to the reuptake of administered GABA by presynaptic neurons and glial cells (Olsen and DeLorey, 1999) and/or rapid clearance of administered GABA after degradation. In the present study, I did not investigate β-Ala, the amino acid composing carnosine together with His, on the sleep/wake effects. Previous studies, however, demonstrated central administrations of β-Ala or the cocktail of β-Ala and His induced hypoactive states in rodents and chicks (Dutra-Filho et al., 1989; Gomez et al., 1978; Tomonaga et al., 2004). In vitro studies suggested that the effect of β-Ala might be caused by an activation of $GABA_A$ receptor and/or glycine receptor by β-Ala (Wu et al., 1993).

The mechanisms for regulations of the observed metabolomic changes in response to increased sleep pressure are still uncertain. All the upstream precursors or downstream products of the differential metabolites did not show significant changes commonly in SD and *Sleepy* mice (Figure 8). There were no changes in the levels of the enzymes which synthesize or degrade the differential metabolites in the previous proteomic/phosphoproteomic analysis (Wang et al., 2018) and RNA-seq analysis

(unpublished data in Yanagisawa/Funato lab). The blood levels of betaine or imidazole dipeptides did not show any significant changes in the same models of enhanced sleep pressure (Suzuki-Abe, unpublished data). Therefore, the observed metabolomic changes would not be caused by the quantitative alterations of synthesizing or degrading enzymes, the alterations of enzymatic activities regulated by protein phosphorylation, or the influx from peripheral blood. The enzymatic activity of carnosine dipeptidase-1, an enzyme hydrolyzing imidazole dipeptides and expressed in the olfactory bulb and hypothalamus in the central nervous system, is decreased by post-translational modifications such as carbonylation and *S*-nitrosylation (Peters et al., 2015). Interestingly, betaine is reported to function reversing certain protein carbonylation (Yoshihara et al., 2021). Therefore, those unstudied molecular interactions could be the key to revealing the mechanisms for regulations of the observed metabolomic changes.

To date, I could not reveal the molecular mechanism for the NREMS-promoting effect of imidazole dipeptides. In my ICV experiments, similar NREMS-promoting effects were observed after the ICV injection of CAR, HMC, and 3mHMC (Figure 5b and 5d). Among the hydrolysis products of HMC, only His but not GABA altered NREMS time in mice (Figure 6b). It suggests the possibility that the NREMS-promoting effect of imidazole dipeptides might be caused by their hydrolyzed product His or its further metabolites. The observation that 3mHMC (hydrolyzed into 3-methyl His) had a similar NREMS-promoting effect also suggests that the pharmacologic effect of His is not caused by its conversion to histamine, a neurotransmitter rather promotes wakefulness (Thakkar, 2011).

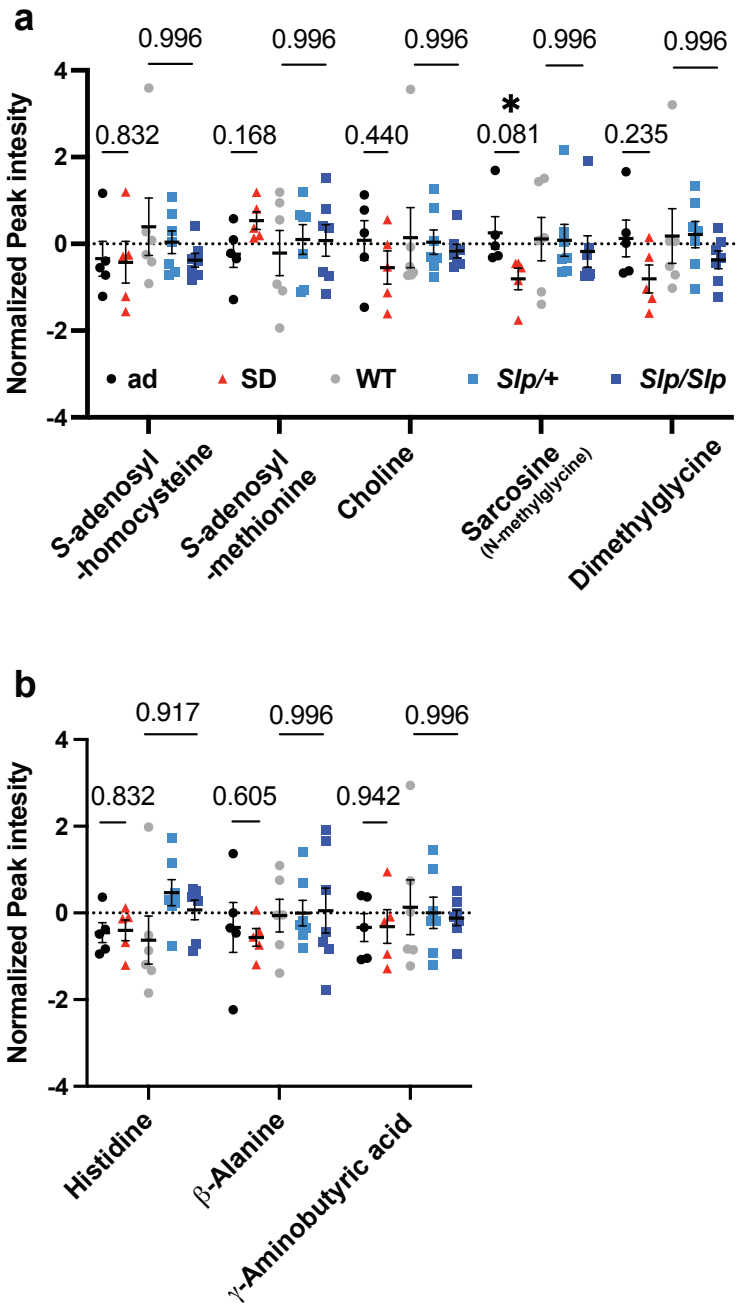

Figure 8. No changes in upstream or downstream metabolites of betaine and imidazole dipeptides.

(a) Quantities of upstream precursors or downstream products of betaine. * $q < 0.1$. Wilcoxon rank sum t-test followed by FDR adjustment (Two-stage linear step-up procedure of Benjamini, Krieger and Yekutieli). Data shown as mean ± SEM.

(b) Quantities of amino acids composing imidazole dipeptides. One-way ANOVA followed by FDR adjustment (Two-stage linear step-up procedure of Benjamini, Krieger and Yekutieli). Data shown as mean ± SEM.

I acknowledge additional limitations in the present study. First, I performed metabolome analyses using the whole-brain samples, since the sleep pressure is thought to involve a wide variety of neural cell types and brain regions in a global manner. Thus, my metabolomic result does not reflect some local changes such as highly regional or cell-type specific alterations, and intracellular/extracellular dynamics of metabolites (Bourdon et al., 2018; Yoon et al., 2019). Second, my pharmacologic experiments using ICV injections do not necessarily mimic the actual brain metabolomic alterations associated with sleep pressure changes.

In summary, my present study identified changes in some specific metabolites associated with elevated sleep pressure. My data also suggest that the major metabolomic changes in SD, the traditional technique to investigate high sleep pressure, could be rather associated with the enforced wakefulness and/or the physical/psychological stress. Furthermore, the ICV administration of imidazole dipeptides, whose levels were increased with elevated sleep pressure, promoted NREMS in mice even when their daily sleep pressure was lowest. The present studies highlight imidazole dipeptides in a potential novel signaling pathway that regulates sleep/wake in response to elevated homeostatic sleep pressure.

References

Bentivoglio, M., Grassi-Zucconi, G., 1997. The Pioneering Experimental Studies on Sleep Deprivation. Sleep 20, 570–576.

Bhat, A., Pires, A.S., Tan, V., Babu Chidambaram, S., Guillemin, G.J., 2020. Effects of Sleep Deprivation on the Tryptophan Metabolism. Int. J. Tryptophan Res. 13, 1178646920970902.

Bjorness, T.E., Dale, N., Mettlach, G., Sonneborn, A., Sahin, B., Fienberg, A.A., Yanagisawa, M., Bibb, J.A., Greene, R.W., 2016. An Adenosine-Mediated Glial-Neuronal Circuit for Homeostatic Sleep. J. Neurosci. 36, 3709–3721.

Bonfanti, L., Peretto, P., De Marchis, S., Fasolo, A., 1999. Carnosine-related dipeptides in the mammalian brain. Prog. Neurobiol. 59, 333–353.

Borbély, A.A., 1982. A two process model of sleep regulation. Hum. Neurobiol. 1, 195–204.

Borbély, A.A., Daan, S., Wirz-Justice, A., Deboer, T., 2016. The two-process model of sleep regulation: a reappraisal. J. Sleep Res. 25, 131–143.

Bourdon, A.K., Spano, G.M., Marshall, W., Bellesi, M., Tononi, G., Serra, P.A., Baghdoyan, H.A., Lydic, R., Campagna, S.R., Cirelli, C., 2018. Metabolomic analysis

of mouse prefrontal cortex reveals upregulated analytes during wakefulness compared to sleep. Sci. Rep. 8, 1–17.

Burd, G.D., Davis, B.J., Macrides, F., Grillo, M., Margolis, F.L., 1982. Carnosine in primary afferents of the olfactory system: an autoradiographic and biochemical study. J. Neurosci. 2, 244–255.

Chong, J., Wishart, D.S., Xia, J., 2019. Using MetaboAnalyst 4.0 for Comprehensive and Integrative Metabolomics Data Analysis. Curr. Protoc. Bioinformatics 68, e86.

Dickinson, M.E., Flenniken, A.M., Ji, X., Teboul, L., Wong, M.D., White, J.K., Meehan, T.F., Weninger, W.J., Westerberg, H., Adissu, H., Baker, C.N., Bower, L., Brown, J.M., Caddle, L.B., Chiani, F., Clary, D., Cleak, J., Daly, M.J., Denegre, J.M., Doe, B., Dolan, M.E., Edie, S.M., Fuchs, H., Gailus-Durner, V., Galli, A., Gambadoro, A., Gallegos, J., Guo, S., Horner, N.R., Hsu, C.-W., Johnson, S.J., Kalaga, S., Keith, L.C., Lanoue, L., Lawson, T.N., Lek, M., Mark, M., Marschall, S., Mason, J., McElwee, M.L., Newbigging, S., Nutter, L.M.J., Peterson, K.A., Ramirez-Solis, R., Rowland, D.J., Ryder, E., Samocha, K.E., Seavitt, J.R., Selloum, M., Szoke-Kovacs, Z., Tamura, M., Trainor, A.G., Tudose, I., Wakana, S., Warren, J., Wendling, O., West, D.B., Wong, L., Yoshiki, A., International Mouse Phenotyping Consortium, Jackson Laboratory, Infrastructure Nationale PHENOMIN, Institut Clinique de la Souris (ICS), Charles River Laboratories, MRC Harwell, Toronto Centre for Phenogenomics, Wellcome Trust Sanger Institute, RIKEN BioResource Center, MacArthur, D.G., Tocchini-

Valentini, G.P., Gao, X., Flicek, P., Bradley, A., Skarnes, W.C., Justice, M.J., Parkinson, H.E., Moore, M., Wells, S., Braun, R.E., Svenson, K.L., de Angelis, M.H., Herault, Y., Mohun, T., Mallon, A.-M., Henkelman, R.M., Brown, S.D.M., Adams, D.J., Lloyd, K.C.K., McKerlie, C., Beaudet, A.L., Bućan, M., Murray, S.A., 2016. High-throughput discovery of novel developmental phenotypes. Nature 537, 508–514.

Dutra-Filho, C.S., Wannmacher, C.M., Pires, R.F., Gus, G., Kalil, A.M., Wajner, M., 1989. Reduced locomotor activity of rats made histidinemic by injection of histidine. J. Nutr. 119, 1223–1227.

Dyar, K.A., Lutter, D., Artati, A., Ceglia, N.J., Liu, Y., Armenta, D., Jastroch, M., Schneider, S., de Mateo, S., Cervantes, M., Abbondante, S., Tognini, P., Orozco-Solis, R., Kinouchi, K., Wang, C., Swerdloff, R., Nadeef, S., Masri, S., Magistretti, P., Orlando, V., Borrelli, E., Uhlenhaut, N.H., Baldi, P., Adamski, J., Tschöp, M.H., Eckel-Mahan, K., Sassone-Corsi, P., 2018. Atlas of Circadian Metabolism Reveals System-wide Coordination and Communication between Clocks. Cell 174, 1571–1585.e11.

Franken, P., Chollet, D., Tafti, M., 2001. The homeostatic regulation of sleep need is under genetic control. J. Neurosci. 21, 2610–2621.

Furuse, M., 2015. The function of carnosine and its homologs on behavior. In: Preedy, V.R. (Ed.), Imidazole dipeptides: chemistry, analysis, function and effects, Royal Society of Chemistry, Cambridge, pp. 471-492.

Gallant, S., Kukley, M., Stvolinsky, S., Bulygina, E., Boldyrev, A., 2000. Effect of carnosine on rats under experimental brain ischemia. Tohoku J. Exp. Med. 191, 85–99.

Goel, N., 2015. “Omics” Approaches for Sleep and Circadian Rhythm Research: Biomarkers for Identifying Differential Vulnerability to Sleep Loss. Current Sleep Medicine Reports 1, 38–46.

Gottesmann, C., 2002. GABA mechanisms and sleep. Neuroscience 111, 231–239.

Hendricks, J.C., Finn, S.M., Panckeri, K.A., Chavkin, J., Williams, J.A., Sehgal, A., Pack, A.I., 2000. Rest in Drosophila is a sleep-like state. Neuron 25, 129–138.

Hughes, M.E., Hogenesch, J.B., Kornacker, K., 2010. JTK_CYCLE: an efficient nonparametric algorithm for detecting rhythmic components in genome-scale data sets. J. Biol. Rhythms 25, 372–380.

International Mouse Phenotyping Consortium, 2021. Gene: CNDP2 MGI:1913304 [WWW Document]. Cndp2 Mouse Gene Details | CNDP dipeptidase 2 (metallopeptidase M20 family). URL https://www.mousephenotype.org/data/genes/MGI:1913304 (accessed 11.10.21).

Irwin, M.R., 2019. Sleep and inflammation: partners in sickness and in health. Nat. Rev. Immunol. 19, 702–715.

Iwasaki, K., Komiya, H., Kakizaki, M., Miyoshi, C., Abe, M., Sakimura, K., Funato, H., Yanagisawa, M., 2018. Ablation of Central Serotonergic Neurons Decreased REM Sleep and Attenuated Arousal Response. Front. Neurosci. 12, 535.

Jain, S., Kim, E.-S., Kim, D., Burrows, D., De Felice, M., Kim, M., Baek, S.-H., Ali, A., Redgrave, J., Doeppner, T.R., Gardner, I., Bae, O.-N., Majid, A., 2020. Comparative Cerebroprotective Potential of d- and l-Carnosine Following Ischemic Stroke in Mice. Int. J. Mol. Sci. 21.

Kaskie, R.E., Graziano, B., Ferrarelli, F., 2017. Schizophrenia and sleep disorders: links, risks, and management challenges. Nat. Sci. Sleep 9, 227–239.

Kiank, C., Zeden, J.-P., Drude, S., Domanska, G., Fusch, G., Otten, W., Schuett, C., 2010. Psychological stress-induced, IDO1-dependent tryptophan catabolism: implications on immunosuppression in mice and humans. PLoS One 5, e11825.

Kubota, K., 1989. Kuniomi Ishimori and the first discovery of sleep-inducing substances in the brain. Neurosci. Res. 6, 497–518.

Lazarus, M., Oishi, Y., Bjorness, T.E., Greene, R.W., 2019. Gating and the Need for Sleep: Dissociable Effects of Adenosine A1 and A2A Receptors. Front. Neurosci. 13, 740.

Mehrazad-Saber, Z., Kheirouri, S., Noorazar, S.-G., 2018. Effects of l-Carnosine Supplementation on Sleep Disorders and Disease Severity in Autistic Children: A Randomized, Controlled Clinical Trial. Basic Clin. Pharmacol. Toxicol. 123, 72–77.

Mena Gomez, M.A., Carlsson, A., Garcia de Yebenes, J., 1978. The effect of beta-alanine on motor behaviour, body temperature and cerebral monoamine metabolism in rat. J. Neural Transm. 43, 1–9.

Miyoshi, C., Kim, S.J., Ezaki, T., Ikkyu, A., Hotta-Hirashima, N., Kanno, S., Kakizaki, M., Yamada, M., Wakana, S., Yanagisawa, M., Funato, H., 2019. Methodology and theoretical basis of forward genetic screening for sleep/wakefulness in mice. Proc. Natl. Acad. Sci. U. S. A. 116, 16062–16067.

Nath, R.D., Bedbrook, C.N., Abrams, M.J., Basinger, T., Bois, J.S., Prober, D.A., Sternberg, P.W., Gradinaru, V., Goentoro, L., 2017. The Jellyfish Cassiopea Exhibits a Sleep-like State. Curr. Biol. 27, 2984–2990.e3.

Ohnishi, T., Balan, S., Toyoshima, M., Maekawa, M., Ohba, H., Watanabe, A., Iwayama, Y., Fujita, Y., Tan, Y., Hisano, Y., Shimamoto-Mitsuyama, C., Nozaki, Y.,

Esaki, K., Nagaoka, A., Matsumoto, J., Hino, M., Mataga, N., Hayashi-Takagi, A., Hashimoto, K., Kunii, Y., Kakita, A., Yabe, H., Yoshikawa, T., 2019. Investigation of betaine as a novel psychotherapeutic for schizophrenia. EBioMedicine 45, 432–446.

Olsen, R.W., DeLorey, T.M., 1999. GABA Synthesis, Uptake and Release. In: Siegel, G.J., Agranoff, B.W., Albers, R.W., Fisher, K.S., Uhler, D.M. (Eds.), Basic Neurochemistry: Molecular, Cellular and Medical Aspects. 6th edition. Lippincott Williams & Wilkins, Philadelphia, https://www.ncbi.nlm.nih.gov/books/NBK27979/

Pang, Z., Chong, J., Zhou, G., de Lima Morais, D.A., Chang, L., Barrette, M., Gauthier, C., Jacques, P.-É., Li, S., Xia, J., 2021. MetaboAnalyst 5.0: narrowing the gap between raw spectra and functional insights. Nucleic Acids Res. 49, W388–W396.

Peng, W., Wu, Z., Song, K., Zhang, S., Li, Y., Xu, M., 2020. Regulation of sleep homeostasis mediator adenosine by basal forebrain glutamatergic neurons. Science 369.

Peters, V., Lanthaler, B., Amberger, A., Fleming, T., Forsberg, E., Hecker, M., Wagner, A.H., Yue, W.W., Hoffmann, G.F., Nawroth, P., Zschocke, J., Schmitt, C.P., 2015. Carnosine metabolism in diabetes is altered by reactive metabolites. Amino Acids 47, 2367–2376.

Raizen, D.M., Zimmerman, J.E., Maycock, M.H., Ta, U.D., You, Y.-J., Sundaram, M.V., Pack, A.I., 2008. Lethargus is a Caenorhabditis elegans sleep-like state. Nature 451, 569–572.

Saper, C.B., Fuller, P.M., 2017. Wake-sleep circuitry: an overview. Curr. Opin. Neurobiol. 44, 186–192.

Schön, M., Mousa, A., Berk, M., Chia, W.L., Ukropec, J., Majid, A., Ukropcová, B., de Courten, B., 2019. The Potential of Carnosine in Brain-Related Disorders: A Comprehensive Review of Current Evidence. Nutrients 11.

Suzuki, A., Sinton, C.M., Greene, R.W., Yanagisawa, M., 2013. Behavioral and biochemical dissociation of arousal and homeostatic sleep need influenced by prior wakeful experience in mice. Proc. Natl. Acad. Sci. U. S. A. 110, 10288–10293.

Suzuki, A., Yanagisawa, M., Greene, R.W., 2020. Loss of Arc attenuates the behavioral and molecular responses for sleep homeostasis in mice. Proc. Natl. Acad. Sci. U. S. A. 117, 10547–10553.

Suzuki-Abe, H., Sonomura, K., Nakata, S., Miyanishi, K., Mahmoud, A., Hotta-Hirashima, N., Miyoshi, C., Sato, T.-A., Funato, H., Yanagisawa, M., 2021. Metabolomic and pharmacologic analyses of brain substances associated with sleep pressure in mice. Neurosci. Res.

Thompson, C.L., Wisor, J.P., Lee, C.-K., Pathak, S.D., Gerashchenko, D., Smith, K.A., Fischer, S.R., Kuan, C.L., Sunkin, S.M., Ng, L.L., Lau, C., Hawrylycz, M., Jones, A.R., Kilduff, T.S., Lein, E.S., 2010. Molecular and anatomical signatures of sleep deprivation in the mouse brain. Front. Neurosci. 4, 165.

Tomonaga, S., Tachibana, T., Takagi, T., Saito, E.-S., Zhang, R., Denbow, D.M., Furuse, M., 2004. Effect of central administration of carnosine and its constituents on behaviors in chicks. Brain Res. Bull. 63, 75–82.

Tsuneyoshi, Y., Yamane, H., Tomonaga, S., Morishita, K., Denbow, D.M., Furuse, M., 2008. Reverse structure of carnosine-induced sedative and hypnotic effects in the chick under acute stress. Life Sci. 82, 1065–1069.

Thakkar, M.M., 2011. Histamine in the regulation of wakefulness. Sleep Med. Rev. 15, 65–74.

Vyazovskiy, V.V., Harris, K.D., 2013. Sleep and the single neuron: the role of global slow oscillations in individual cell rest. Nat. Rev. Neurosci. 14, 443–451.

Wang, Z., Ma, J., Miyoshi, C., Li, Y., Sato, M., Ogawa, Y., Lou, T., Ma, C., Gao, X., Lee, C., Fujiyama, T., Yang, X., Zhou, S., Hotta-Hirashima, N., Klewe-Nebenius, D., Ikkyu, A., Kakizaki, M., Kanno, S., Cao, L., Takahashi, S., Peng, J., Yu, Y., Funato, H.,

Yanagisawa, M., Liu, Q., 2018. Quantitative phosphoproteomic analysis of the molecular substrates of sleep need. Nature 558, 435–439.

Wang-Eckhardt, L., Bastian, A., Bruegmann, T., Sasse, P., Eckhardt, M., 2020. Carnosine synthase deficiency is compatible with normal skeletal muscle and olfactory function but causes reduced olfactory sensitivity in aging mice. J. Biol. Chem. 295, 17100–17113.

Waite, F., Sheaves, B., Isham, L., Reeve, S., Freeman, D., 2020. Sleep and schizophrenia: From epiphenomenon to treatable causal target. Schizophr. Res. 221, 44–56.

Wu, F.-S., Gibbs, T.T., Farb, D.H., 1993. Dual activation of GABAA and glycine receptors by β-alanine: inverse modulation by progesterone and 5α-pregnan-3α-ol-20-one. Eur. J. Pharmacol. Mol. Pharmacol. 246, 239–246.

Yamamoto, H., Fujimori, T., Sato, H., Ishikawa, G., Kami, K., Ohashi, Y., 2014. Statistical hypothesis testing of factor loading in principal component analysis and its application to metabolite set enrichment analysis. BMC Bioinformatics 15, 51.

Yamamoto, H., 2017. PLS-ROG: Partial least squares with rank order of groups. J. Chemom. 31, e2883.

Yamamoto H., 2019. pls-rog. GitHub repository. https://github.com/hiroyukiyamamoto/pls-rog

Yokogawa, T., Marin, W., Faraco, J., Pézeron, G., Appelbaum, L., Zhang, J., Rosa, F., Mourrain, P., Mignot, E., 2007. Characterization of sleep in zebrafish and insomnia in hypocretin receptor mutants. PLoS Biol. 5, e277.

Yoon, S.J., Long, N.P., Jung, K.-H., Kim, H.M., Hong, Y.J., Fang, Z., Kim, S.J., Kim, T.J., Anh, N.H., Hong, S.-S., Kwon, S.W., 2019. Systemic and Local Metabolic Alterations in Sleep-Deprivation-Induced Stress: A Multiplatform Mass-Spectrometry-Based Lipidomics and Metabolomics Approach. J. Proteome Res. 18, 3295–3304.

Yoshihara, S., Jiang, X., Morikawa, M., Ogawa, T., Ichinose, S., Yabe, H., Kakita, A., Toyoshima, M., Kunii, Y., Yoshikawa, T., Tanaka, Y., Hirokawa, N., 2021. Betaine ameliorates schizophrenic traits by functionally compensating for KIF3-based CRMP2 transport. Cell Rep. 35, 108971.

Acknowledgments

I also thank all members of the Sato laboratory, Yanagisawa/Funato laboratory, and WPI-IIIS. Especially I would like to show my best gratitude to Dr. K. Sonomura from Shimadzu corporation for a great deal of cooperation and active discussion, to Dr. M. Yanagisawa, Dr. H. Funato, Dr. TA. Sato for the supervision, and to Dr. C. Miyoshi, Ms. N. Hotta-Hirashima, for their kind support and advice on this project.

Also, I would like to give my special thanks to family members, my parents Shizuka and Kaori Suzuki, my brothers Wataru Suzuki, and my grandparents Toshio and Harumi Abe. My last name shown on the cover is a combination of my father's and mother's maiden names to distinguish me from other researchers with the same name.